Study on Heat Transfer Inside a Blocked Region of a Rod Bundle During a LOCA - Model and Experimental Approach

Juan-David Peña-Carrillo, Tony Glantz, Georges Repetto, Alexandre Labergue, Michel Gradeck

STUDY ON HEAT TRANSFER INSIDE A BLOCKED REGION OF A ROD BUNDLE DURING A LOCA –EXPERIMENTAL AND MODEL APPROACH

J-D. Peña Carrillo, T. Glantz, G. Repetto
Institut de Radioprotection et de Sureté Nucléaire, IRSN
Cadarache, Saint Paul lez Durance, France
juan-david.penacarillo@irsn.fr; tony.glantz@irsn.fr georges.repetto@irsn.fr

M. Gradeck, A. Labergue
LEMTA, UMR CNRS 7563, Université de Lorraine, 2 avenue de la forêt de Haye, 54505
Vandoeuvre les Nancy, France
michel.gradeck@univ-lorraine.fr; alexandre.labergue@univ-lorraine.fr

ABSTRACT

This study focuses on the coolability of a partially deformed fuel assembly of a PWR reactor through an accident causing the loss of coolant primary (LOCA). Beyond the dryout point during the reflooding phase, the core is cooled mainly by the flow of superheated vapor and dispersed droplets. The thermal-hydraulic features of this two-phase flow, as well as the damaged cladding characteristics (blockage ratio, blockage length), are important parameters to estimate the heat exchanges and nuclear core coolability through the fuel assemblies.

In order to analyze experimentally the influences of the cladding deformation on the heat transfer, a simplified set-up is proposed to validate recent models. The droplets are produced by a piezoelectric injector generating single and calibrated ones while a superheated vapor flow comes from a vapor generator. This mixing is injected in different vertical tubes, which internal hydraulic diameters are equivalent to real, deformed or not, sub-channel PWR. So, different blockage scenarios are studied in order to evaluate the different heat transfer mechanisms. The test section is heated up to a representative temperature of the fuel rod during a LOCA (>600°C). Upstream and downstream of the blocked zone, measurements will be carried out using optical measurement techniques such as Phase Doppler Anemometry (PDA) and Laser Induced Fluorescence (LIF) to characterize the droplet's flow. Along this zone, temperature measurements of the tube surface will be performed using infrared thermography. So, a heat transfer balance can be done to estimate the contributions of vapor and droplet cooling.

For the purpose of performing the pre-calculation of the tests foreseen in the set-up, a one-dimensional model taking into account of the heat transfers mechanism in a post-dryout region is developed in the present paper. This model which integrates conservation of mass and energy, droplet momentum, as well as a system of transport equations, will allow estimating the respective impact of the different heat transfer mechanisms involved during the cooling.

KEYWORDS
Coolability, blockage, LOCA, Heat transfer, LIF, PDA

1. INTRODUCTION

One of the design-related accidents of a PWR reactor is the LOCA (Loss Of Coolant Accident). The initiating event of such an accident is a breach on the primary circuit of the reactor resulting in a loss of water inventory, and consequently in a drying of the fuel assemblies. As a result, a considerable increase in temperature would occur within the core of the reactor. Thus, the fuel rod claddings may possibly deform

and blocked zones can appear (Figure 1a). During the reflooding phase, three zones can be identified depending on the type of flow: (i) the quench front corresponding to the predominantly liquid water zone when the first boiling mechanisms are observed; (ii) a two-phase post-dryout zone composed of superheated vapor and dispersed droplets. Finally, when all the droplets disappear because of the evaporation, (iii) a monophasic post-dryout zone of superheated vapor. The coolability of the core during the reflooding by the emergency cooling backup systems (ECCS) is a complex thermal-hydraulic phenomenon which depends on the thermal-hydraulics features of the flow and the damaged cladding characteristics (blockage ratio, blockage length).

The French Safety Institute "Institut de Radioprotection et de Sureté Nucléaire" (IRSN) has launched, with the support of ANR, the PERFROI project [1][2] for a six year period (2014-2019) which is structured in two axes: thermal mechanics (axis 1) and thermal hydraulics (axis 2). The COAL experiments (in the axis 2), focuses on the outstanding issue of the coolability of a partially deformed fuel assembly, in particular, the study of the thermal hydraulic behavior of the ballooned area, during reflooding phase by water injection with the safety systems. To understand and analyze LOCA, a new set-up is built at the Laboratory for Energy, Theoretical and Applied Mechanics (LEMTA) to simulate close LOCA conditions. It will focus on the characterization of two-phase flows with heat and mass transfer in blocked structures at representative sub-channel scales. The use of specific instrumentation such as Laser Induced Fluorescence (LIF), Phase Doppler Anemometry (PDA) and infrared Camera (IR) technics will help to perform accurate balances, particularly those concerning heat and mass.

In order to perform the pre-calculation of the tests foreseen in the set-up and to obtain a first theoretical approach to the cooling, a one-dimensional mechanistic model will be presented in this paper for two-phase flow taking into account the different mechanisms of heat and mass transfers in a post-dryout zone (Forced convection, radiation and the impact of drop onto the tube surface in the Leidenfrost regime). This model is based on a set of conservation equation (mass and energy, droplet momentum) coupled to transport equations. A set of closure relations will allow estimating the respective impact of the different heat transfer mechanisms involved in the cooling.

2. EXPERIMENTAL APPROACH

Within the frame of the thermal hydraulic axis of PERFROI project, an experimental study has been launched in 2016 focusing on the characterization of two-phase flows across a representative blocked sub-channel of a damaged assembly for different LOCA configurations. The proposed approach is expected to validate the models already developed on flow and heat transfer between wall and fluid and mainly understand and quantify the heat transfer between the dispersed two-phase flow and the heated walls.

The experimental test section is a vertical tube made of Inconel-625 (Nickel and chrome alloy with a low degree of oxidation at high temperatures). In order to reproduce the geometry of the partially blocked zones, a typical Venturi configuration was chosen: an internal diameter of the tube upstream and downstream of 11.78 mm, equivalent to the hydraulic diameter of a non-deformed representative sub-channel ($D_h=4P_c/S_{nbal}$). A sub-channel is defined as the fluid domain between four adjacent fuel rods. The blockage ratio is defined as ($1-S_{bal}/S_{nbal}$). The constricted section of the Venturi tube will have an internal diameter equivalent to the hydraulic diameter of a deformed representative sub-channel (Figure 1). The angle of the convergent and divergent part of the venturi is 6° in the present study. Different ratios and lengths of ballooning will be studied (See Table I)

2.1 Experimental procedure

The partially blocked section of the tube is heated up to 800 °C by Joule effect using an electric generator (TDK Lambda Genesys2U series GEN 10-330), the temperature is controlled in real time using an infrared camera device. When the operating temperature is reached, the injection of the two-phase flow is started.

Table I. Geometrical configurations of the partially blocked section to be tested

	Config. n°1	Config. n°2	Config. n°3	Config. n°4	Config. n°5
Blockage ratio	0%	61%	61%	90%	90%
Equivalent hydraulic diameter	11.78 mm	7.35 mm	7.35 mm	3.72 mm	3.72 mm
Height of the ballooned area	-	100 mm	300 mm	100 mm	300 mm
Thickness	0.57 mm	0.86 mm	0.86 mm	1.38 mm	1.38 mm

The superheated vapor/droplet flow is injected upstream of the tube. The vapor flow is produced using a vapor generator (AURA MA-6 kW®) able to produce vapor at a maximum temperature of 180 °C and a maximum mass flow rate of 8,4 kg/h; At the outlet of the vapor generator, a superheater can increase their temperature up to 300°C (AURA S2000 - 2 kW®). The dispersed phase is produced by a piezoelectric injector (FMP Technology®) able to generate calibrated drops at diameters up to 500 µm at different frequencies. The range of thermal hydraulics parameters able to study in the present test facility is shown in Table II

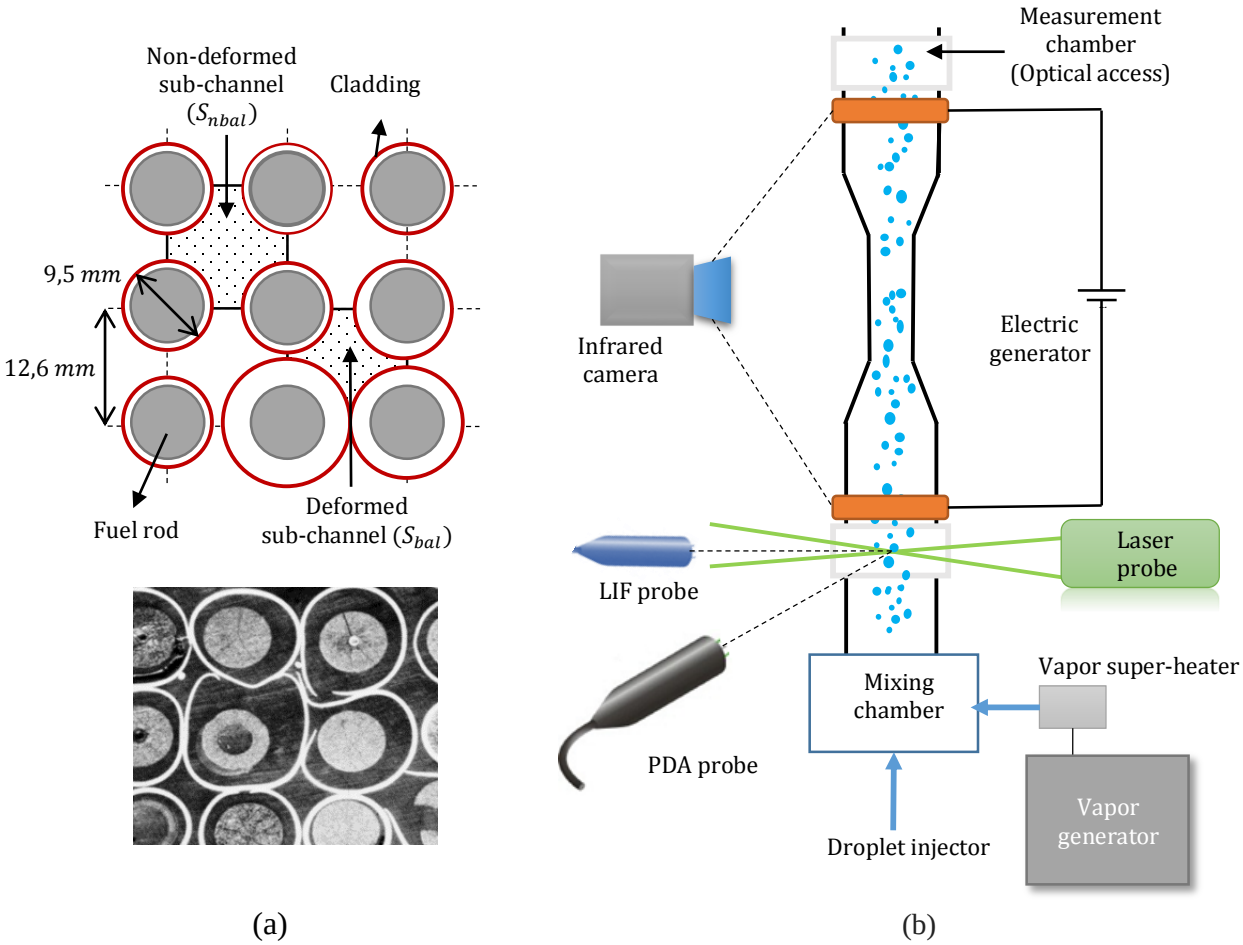

(a) (b)

Figure 1. (a) Representation of a partial damaged PWR fuel assembly, Phebus LOCA experiments (1983) ; (b) Scheme of thermal-hydraulic circuit of the experimental test facility

Measurements of the droplet characteristics are carried out upstream and downstream the constricted section of the tube: A Phase Doppler Anemometry technique (Dantec Dynamic® - classic PDA) is used to

measure diameter, axial velocity, and probability distribution function PDF of droplets. Using the laser-induced fluorescence (LIF) thermometry based on the thermodependance of a fluorescent dye previously seeded in the liquid.. The temperature of the superheated vapor is also measured upstream and downstream of the tube via insulated thermocouples. An infrared camera is used to measure the axial temperature field of the outside tube surface and to estimate the total wall to fluid heat transfer. The transient cooling of the tube is analyzed by performing coupled measurements of LIF, PDA, and infrared camera [3]

Table II. Thermal hydraulic conditions for the present test facility

Inlet vapor flow mass	Up to 8.4 Kg/h
Inlet vapor temperature	180°C - 300°C
Inlet droplet velocity	Up to 10 m/s
Inlet droplet temperature	From 25°C to saturation temperature
Cladding temperature before reflooding	600°C to 800°C
Electric power supply	Up to 3,3 kW

2.2 Experimental diagnostics

- **Phase Doppler Anemometry PDA:**

The properties of dispersed flow (diameter, z-axis velocity, and probability distribution function PDF) are performed using a Phase Doppler system (PDA). The Phase Doppler system is a 2D commercial classic PDA manufactured by Dantec-Dynamics®. PDA excitation volume is formed by the intersection of two laser beams coming from an argon laser source, ($\lambda = 514.5$nm). The system includes a classic PDA receiver which operates in the first refraction mode. Finally, the signal is analyzed with the use of a P80 signal processor.

- **Infrared camera:**

The temperature along the constricted section of the tube is estimated thanks to an infrared camera. The infrared camera (Cedip® Jade III) is built with a focal plane array photonics detectors (InSb) working in the spectral range [3–5 μm] and it's equipped with a narrow-bandwidth [3.97–4.01 μm] spectral filter to fit with the expected experimental temperature range. The spatial resolution is 320x240 pixels/ frame. A measurement using a thermocouple is required for the calibration of the detector. A thermocouple is used to provide a reference temperature: this measurement is required to calibrate the whole measurement chain. The calibration is performed by heating the tube up to 800 °C and by recording simultaneously the infrared signal and the temperature measured by the thermocouple, while the tube is cooled naturally (radiative, convective heat transfer and residual conduction).

- **Laser Induced fluorescence (LIF):**

The temperature of the droplets is performed using the LIF technique. This technique is based on the measurement of the fluorescence intensity of a temperature-sensitive fluorescent dye at a low concentration. For this case, sulforhodamine B is used because of its temperature sensibility and for its solubility in water. The fluorescence is induced by the green line of an argon ion laser, the same used for PDA measurement. The theoretical explanation of this technique, as well as different examples of application for the case of temperature measurement in poly-dispersed flows of droplets, can be found in [3][4][5]

3. MODEL APPROACH

The following study will provide a theoretical approach of the thermal-hydraulic behavior of the two-phase flow inside the tube. The present model, composed of conservation of mass, droplet momentum, and conservation of energy, as well as a system of transport equations, will allow estimating the respective impact of the different heat transfer mechanisms involved across the channel. In order to simplify the calculation, the following assumptions are made:

- One-dimensional flow
- Droplets are at saturation temperature
- Liquid droplets have a spherical shape
- No droplet break-up and coalescence
- No vapor flow separation in the expansion area

3.1 Heat transfers mechanisms in post-dryout region

As shown in figure 1, six heat transfers mechanisms in the post-dryout region are of major importance in the analyses of dispersed flows. Several prediction methods of these heat transfers mechanism are proposed in the literature. The correlations used in the present model will be presented below:

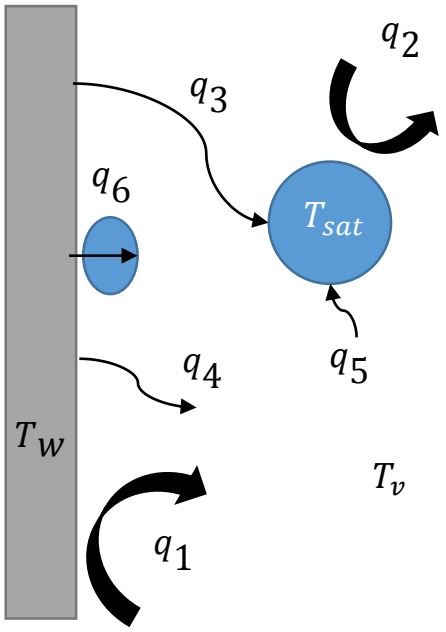

Figure 2. Heat transfers mechanisms in post-dryout region for a two-phase flow

Wall to vapor forced convection (q_1): The heat flux extracted at the wall by the vapor can be expressed as follows

$$q_1 = h_1(T_w - T_v) \tag{1}$$

Gnielinski [6] proposes a model predicting the heat transfer coefficient h_1:

$$h_1 = \left(\frac{\lambda_v}{D_h}\right)\frac{\left(\frac{f_f}{8}\right)(Re - 1000)Pr}{1 + 12{,}7\left(\frac{f_f}{8}\right)^{0{,}5}\left(Pr^{\frac{2}{3}} - 1\right)}\left(\frac{T_v}{T_w}\right)^{0.45} \tag{2}$$

Vapor to droplet interfacial convection (q_2): The interfacial vapor to droplet heat flux can be expressed as follows:

$$q_2 = h_2(T_v - T_d) \tag{3}$$

Experimentally, it has been shown that the evaporation decreases the heat transfer between vapor and drops[7][8]. To take into account this, Kim's correlation [9]is used:

$$h_2 = \left(\frac{\lambda_v}{d_d}\right)\frac{2 + 0.74Re^{0.5}Pr^{\frac{1}{3}}}{1 + B_T} \tag{4}$$

Where Re is based on the droplet diameter and B_T is the mass transfer number defined as:

$$B_T = \frac{\tilde{h}_g(T_v) - \tilde{h}_l(T_d)}{\tilde{h}_g(T_d) - \tilde{h}_l(T_d)} \tag{5}$$

Wall to fluid and fluid to fluid radiation (q_3, q_4, and q_5): The heat flux exchanged between the wall and the two-phase flow is a coupled phenomenon that takes into account the optical, geometric and thermal properties of each medium. In order to estimate these contributions, and considering a gray and diffuse mixture of vapor-droplets in the optically thin regime, the Sun's model [10] is used in the present work to characterize the thermal radiation:

$$q_3 = \varphi_{w-d}\sigma_b\left(T_w^4 - T_d^4\right) \tag{6}$$

$$q_4 = \varphi_{w-v}\sigma_b(T_w^4 - T_v^4) \tag{7}$$

$$q_5 = \varphi_{v-d}\sigma_b\left(T_v^4 - T_d^4\right) \tag{8}$$

Where φ is the gray-body factor, and depends on the emissivity of the medium and the wall and can be estimated using the following equation:

$$\varepsilon_v = 1 - e^{-a_v D_h} \tag{9}$$

$$\varepsilon_d = 1 - e^{-a_d D_h} \tag{10}$$

In our case, the wall emissivity is 0.6. The vapor emissivity, taking into account the assumption of an optically thin medium, can be estimated directly using one of the correlations given by Siegel [11]. The droplet absorption coefficient (a_d) is given using the following equation [10]

$$a_d = \frac{1.12\alpha_d}{d_d} \tag{11}$$

Wall to droplet direct contact heat transfer (q_6): Since the wall temperature is above the Leidenfrost temperature, a vapor layer still exists between the droplet and the wall when it impinges the wall. Also, for low Weber numbers, characteristic of LOCA condition (below a critical value of the order of 30), a pure rebound phenomenon without droplet break-up can be observed. Guo [12] developed a model to account for the heat transfer between by conduction between the wall and the droplet through the vapor layer:

$$q_6 = (T_w - T_{sat})\left(\frac{18\lambda_v^3 t_r^3 \rho_v L_v \dot{m}_{dep}^5}{d_d^5 \rho_v^4 \mu_v \alpha_d (T_w - T_{sat})}\right)^{\frac{1}{4}} \tag{12}$$

The deposition model of Hewitt [13] is used in this work to calculate the droplet deposition rate m_{dep} :

$$\dot{m}_{dep} = \begin{cases} \dfrac{0.18\alpha_d\rho_d}{\sqrt{\dfrac{\rho_d D_h}{\gamma}}} & if \quad \dfrac{\alpha_d\rho_d}{\rho_v} < 0.3 \\ \dfrac{0.083(\alpha_d\rho_d)^{0.35}}{\sqrt{\dfrac{\rho_d D_h}{\gamma}}}(\rho_v)^{0.65} & if \quad \dfrac{\alpha_d\rho_d}{\rho_v} \geq 0.3 \end{cases} \tag{13}$$

With t_r the droplet residence time suggested as:

$$t_r = \pi\sqrt{\frac{\rho_d d_d^3}{8\gamma}} \tag{14}$$

3.2 Momentum balance of droplets

Because of the high droplet density compared to the vapor phase, the droplets are accelerated mainly by the effect of the drag force (added mass force neglected). Thus, the following correlation allows to calculate the z-axis evolution of the droplet velocity:

$$u_d\rho_d\frac{du_d}{dz} = -\frac{3}{4d_d(1+B_T)}\theta C_d\rho_v(u_d-u_v)|(u_d-u_v)| + (\rho_v-\rho_d)g \tag{15}$$

Where C_d is the drag coefficient of an isolated droplet. The correlation of Morsi [14] allows to estimate it in the following way:

$$C_d = \frac{A_1}{Re} + \frac{A_2}{Re^2} + A_3 \tag{16}$$

A1, A2, and A3 are constants which depend on Reynolds number based on the droplet diameter.

As in the case of the calculation of h2, the drag coefficient is reduced by the evaporation effect $1/(1+B_T)$.The coefficient θ, correct the drag coefficient of an isolated droplet taking into account the influence of the dispersed phase concentration [15]:

$$\theta = \frac{1}{1-6.55\alpha_d} \tag{17}$$

3.3 Energy balance of vapor

In order to estimate the increase in vapor temperature, a conservation of energy balance is performed:

$$\Delta T_v = \left(\frac{Q_1+Q_4-(Q_2+Q_5)}{C_{p,v}(\dot{m}_v+\dot{m_{ev}})} - T_v\left(1-\frac{\dot{m}_v}{\dot{m}_v+\dot{m_{ev}}}\right)\right) \tag{18}$$

Where $\dot{m_{ev}}$ is the evaporated droplet mass flux.

3.4 Transport equations

In order to estimate the axial evolution of important volumetric parameters (i.e. volumetric interfacial area a_{int}, volumetric liquid fraction α_d) the transport equation for ηth moment density is defined as [16]:

$$\frac{d}{dt}(S_\eta) + \nabla.(S_\eta u_{d,\eta}) = \eta S_{\eta-1}G_{\eta-1} + \omega_\eta \tag{19}$$

The first term on the RHS represent the change in volume of droplets (Due to evaporation for our case) and the second term, ω_η, the source term due to droplet break-up and coalescence. Assuming only one direction (z-axis), and neglecting the break-up and coalescence we obtain:

$$\frac{d}{dt}(S_\eta) + \frac{d}{dz}(S_\eta u_{d,\eta}) = \eta S_{\eta-1} G_{\eta-1} \tag{20}$$

S_η, $u_{d\eta}$, and G_η are defined as[16]:

$$\begin{aligned} S_\eta &= n \int_0^\infty P(d)\, d^\eta \; dd \\ u_{d,\eta} &= \frac{\int_0^\infty P(d)\, u_d(d)\, d^\eta \; dd}{\int_0^\infty P(d) \; d^\eta \; dd} \\ G_\eta &= \frac{\int_0^\infty P(d)\, \dot{G}(d)\, d^\eta \; dd}{\int_0^\infty P(d) \; d^\eta \; dd} \end{aligned} \tag{21}$$

Where P(d) is the droplet diameter distribution function (PDF), n denotes the droplet concentration (Number of droplets per unit volume), u_d is the droplet velocity and $\dot{G}$, is the particle size change due to evaporation (dd/dt, (m/s)); in order to estimate G_η, the following correlation is used:

$$\dot{G}(d) = b_1 . d_d^{b_2} \tag{22}$$

Where b_1 and b_2 are constants which depend on the local thermal-hydraulic features. Making successively η=0,1,2,3 in equation (21), four transport equations allow to solve S_0, S_1, S_2, and S_3. Thus n, a_i and α_d can be determined ($n = S_0$; $a_{int} = \pi S_2$; $\alpha_d = \pi S_3/6$)

3.5 Droplet diameter distribution (PDF)

A log-normal distribution is adopted in the present work, as suggested by [17]:

$$P(d) = \frac{1}{\sqrt{2\pi}\sigma d} e^{\left(- \frac{\left(\ln\left(\frac{d}{d_{oo}}\right)\right)^2}{2\sigma^2} \right)} \tag{23}$$

Where σ, is the standard deviation of the natural logarithm and d_{oo} the mean characteristic diameter. Thus, it is possible to define the PDF at any point of the tube by knowing only these two parameters which depend on the first and second-moment densities, as well as α_d calculated using the equation (21):

$$\begin{aligned} \sigma &= \sqrt{\ln\left(\frac{6\alpha_d S_1}{\pi S_2^2}\right)} \\ d_{oo} &= \frac{6\alpha_d}{\pi S_2} e^{-\frac{5}{2}\sigma^2} \end{aligned} \tag{24}$$

Discretization of PDF function [18]

In order to consider the droplet distribution in heat transfer calculations, the PDF is divided into bins of equal volume (Figure 3). The equations presented in subsections 3.1, 3.2 et 3.3 are solved for each bin using the volumetric liquid fraction ($\alpha_{d,i} = \alpha_d/N_{bins}$) and the equivalent bin Sauter diameter, defined as:

$$d_{32,i} = \frac{\int_{d_{low,i}}^{d_{up,i}} P(d)\, d_d^3 dd}{\int_{d_{low,i}}^{d_{up,i}} P(d)\, d_d^2 dd} \tag{25}$$

Thus, total heat transfer contribution at a given axial position can be calculated as:

$$q_j = \sum_{i=1}^{N_{bins}} q_{j,i} \tag{26}$$

With $q_{j,i}$, the heat transfers flux mechanisms of the dispersed phase for each bin (i.e. $q_{2,i}$, $q_{3,i}$, and $q_{6,i}$)

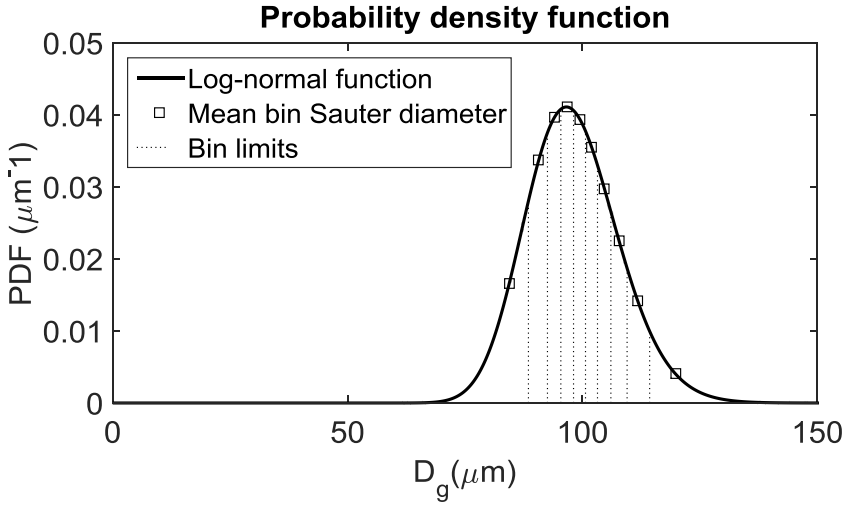

Figure 3. Log-normal distribution for σ=0.10 and d_{oo}=100 μm. 10 bins

4. MODEL APPLICATION

4.1 Geometry and flow features

In this paper, a vertical tube of 0.5 m long is considered. Configurations 1, 3, and 5 will be analyzed from Table I (I.e. blockage ratio 0%, 61% and 90% for a blockage length of 0.3 m). A temperature of 800°C is used as wall boundary condition. At the inlet of the domain, the next conditions are imposed:

Table III. Thermal-hydraulic conditions at the bottom inlet of the domain

Droplet Velocity (m/s)	Vapor Velocity (m/s)	Droplet Temperature (°C)	Vapor Temperature (°C)	Volumetric Droplet fraction	σ	d_{oo} (m)	P (bar_a)	N_{bins}
10	12	T_{sat}	250	0.001	0.10	$1x10^{-4}$	2	10

4.2 Results and discussions

Two-phase flow characteristics

Figure 4a shows the vapor temperature axial evolution for three different blockage ratios. Vapor temperature is more important when the blockage ratio increases. Upstream the contracted zone, the vapor undergoes a small reduction in temperature because of a large part of its energy is transferred to the dispersed droplet phase for its evaporation, product of a local increase of the volumetric droplet fraction in

the convergent part of the venturi tube (z=0.12 m). In the case of a non-blocked tube (0%), the temperature increases progressively due to an increase in the mass vapor flux produced by the contribution of the evaporation of the dispersed phase, causing a vapor acceleration and improving mainly the wall to vapor heat transfer. In the case of the 61% and 90% blockage, the increase in temperature is mainly due to the change of internal diameter in the intermediate part of the tube and, as a result, high velocities are expected in the contracted part improving the total wall to vapor heat transfer. The vapor velocity also changes in function of the vapor temperature due to the vapor thermo-dependence.

Figure 4b shows the volumetric droplet fraction α_d axial evolution. In the case of a non-blocked tube, a reduction of the droplet fraction is produced by the loss in volume of the dispersed flow due to the evaporation. For the two blockage configurations analyzed, the droplet fraction increases in the contracted zone and decreases downstream.

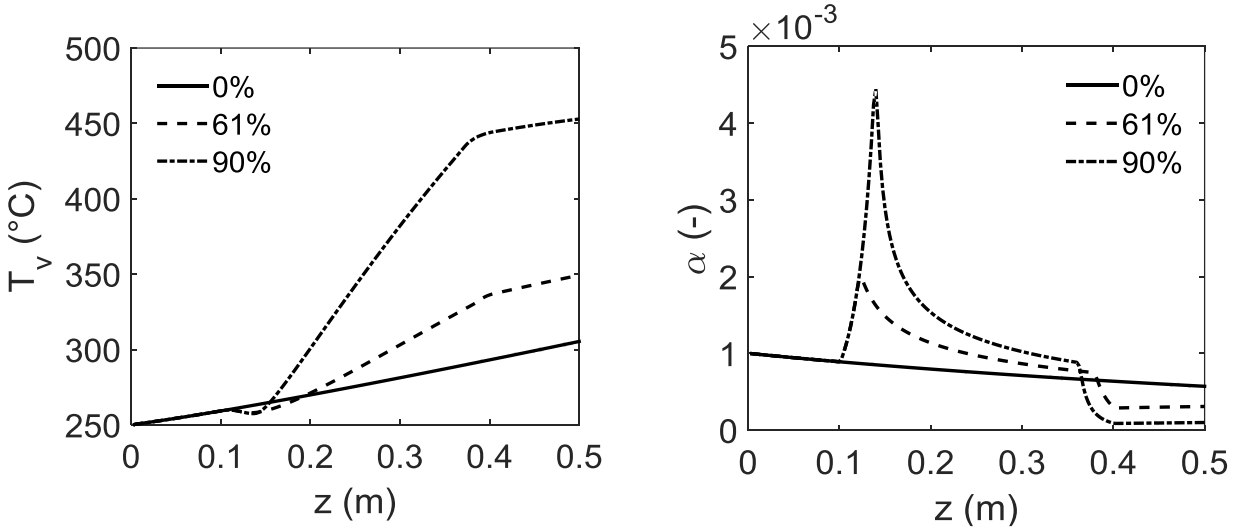

Figure 4. From left to right: Longitudinal evolution of vapor temperature; longitudinal evolution of volumetric droplet fraction

The axial evolution of d_{oo} (Log-normal mean characteristic diameter) is shown in Figure 5a. For the three cases analyzed here, d_{oo} decreases as would be expected because of the droplet evaporation. The diameter decreases more in the case of non-blockage because the droplets are less accelerated compared to blocked configurations, thus the dispersed flow takes more time to cross the domain and the evaporated mass flux is more important. As shown in Figure 5b, droplet evaporation causes an increase in the vapor mass flow of 21%, 19%, and 17% for a blockage ratio of 0%, 61%, and 90% respectively.

Figure 6 shows the probability distribution function of droplets upstream and downstream for a non-blocked tube (0%). As would be expected, the downstream PDF moves towards the left compared to the upstream PDF due to the evaporation of the drops, an effect that reduces its diameter. The mean characteristic diameter d_{00} is reduced from 100 μm to 92 μm, while the standard deviation σ changes only from 0.1 to 0.103. Similar displacement of the PDF toward the left was obtained for the configurations of 61% and 90% blockage.

Heat transfers

In order to analyze the different heat transfer mechanisms, wall to fluid heat transfers for 0% and 61% blockage are shown in
Figure 7. The most important heat transfer contribution along the tube is wall to vapor forced convection (q1). For the non-blocked case, q_1 increases due to the evaporated flux mass and also by thermo-dependency

of superheated vapor which causes an increasing in vapor velocity; For the case of 61% blockage ratio, the contribution of q_1 is much more highlighted due to the significant increase in the vapor velocity because of the change of internal diameter in the intermediate part of the tube. Wall to droplet radiation q_3 plays an important role and its axial evolution is related to the volumetric liquid fraction. Wall to vapor radiation q_4 has also an important contribution, it remains almost constant for a non-blocked tube and is reduced a little in the blocked region. For our study case, wall to droplet direct contact heat transfer q_6 is the smallest wall to fluid contribution. As well as q_3 contribution, q_6 is highly related to the volumetric droplet fraction; Even if this contribution could be neglected, their consideration is important in situations where α_d is higher.

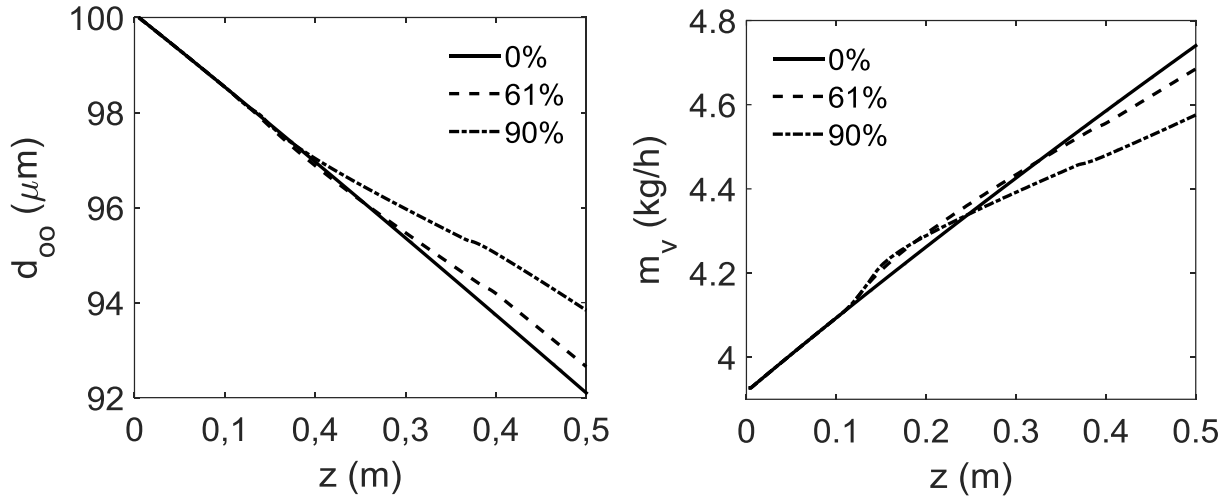

Figure 5. From left to right: Longitudinal evolution of characteristic log-normal diameter d_{oo}; longitudinal evolution of vapor flux mass

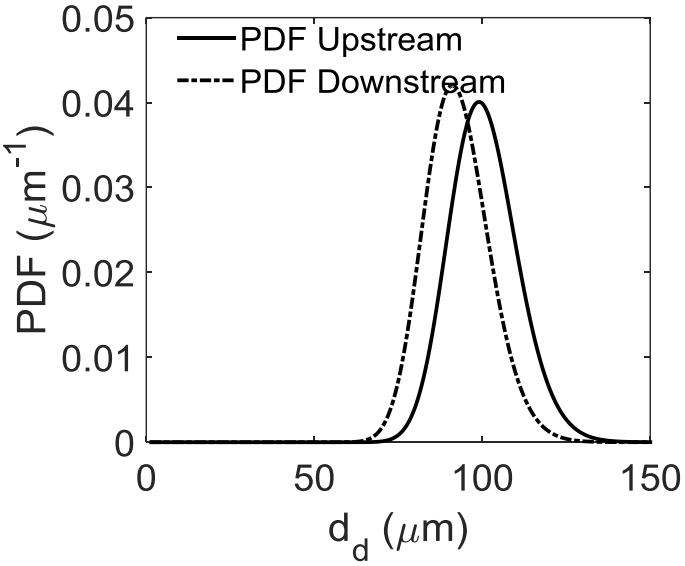

Figure 6. PDF of the droplet diameter upstream and downstream the tube, non-blocked configuration

For the purpose of comparing the different heat transfer mechanisms, the spatial-averaged heat transfer is defined is used and as:

$$\widetilde{q_i} = \frac{1}{L}\int_0^L q_i(z)dz \tag{27}$$

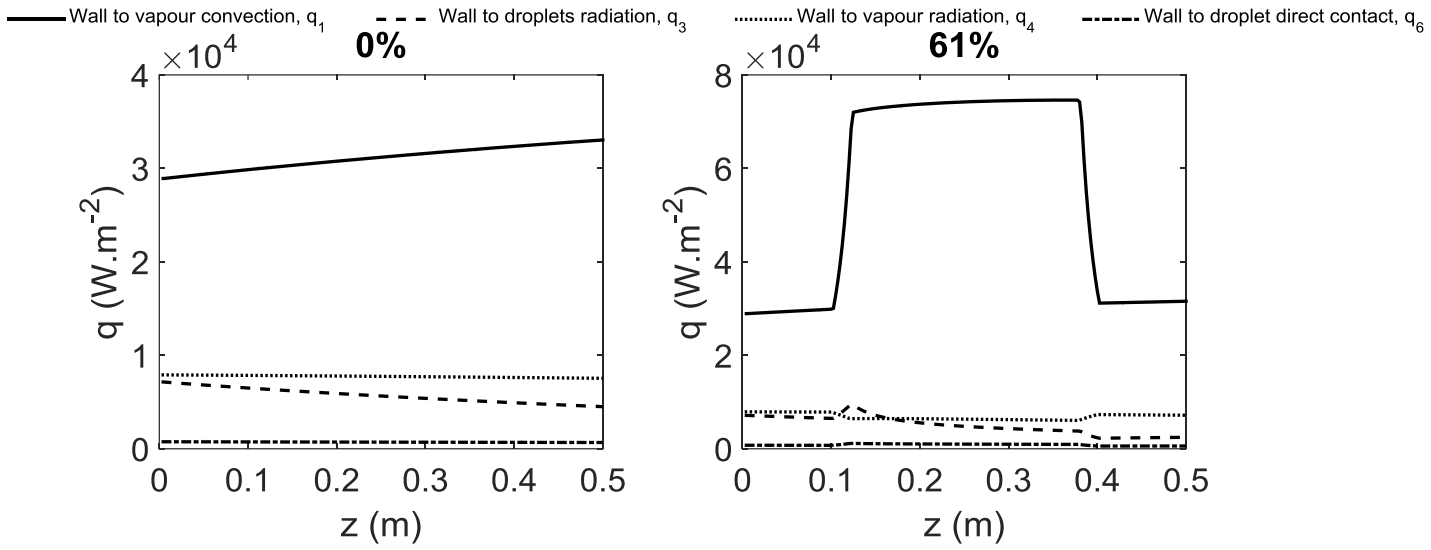

Figure 7. Longitudinal evolution of wall to fluid heat transfers. From left to right: Configuration 1, configuration 3

Table IV shows the spatial-averaged heat transfers of each heat transfer contribution. For all the configuration tested, wall to vapor convective heat transfer q_1 is the most important contribution. This contribution increase as the blockage ratio is more critical representing approximately 68%, 80% and 92% of the total heat flux removed from the wall for configuration 1, 3, and 5 respectively. In fact, the vapor acceleration increases the Reynolds number resulting in an enhancement of the convective heat transfer coefficient h_1. Wall to fluid radiation (i.e q_3 and q_4), decreases as the blockage ratio is more critical. Their contributions represent 30%, 18% and 7% the total heat flux for configurations 1, 3, and 5 respectively. Wall to droplet direct contact heat transfer q_6 increases a little bit as a function of blockage ratio. Their contribution represents 1.5%, 1.2% and 0.8%. Vapor to droplet heat transfer (q_2) which participates mainly in the evaporation of droplets phenomena, is more important as a function of the blockage ratio because the relative velocity between the two phases is more important as well as the vapor temperature. For all the cases, vapor to droplets radiation (q_5) is very small in quantity.

Table IV. Spatial-averaged wall to fluid heat transfer and vapor to droplet heat transfer (Equivalent heat transfer per unit wall area)

	Wall to fluid heat transfer (kW.m^{-2})				**Vapor to droplet heat transfer (kW.m^{-2})**	
	q_1	**q_3**	**q_4**	**q_6**	**q_2**	**q_5**
Configuration 1 (0%)	31.12	5.78	7.74	0.71	24.65	0,025
Configuration 3 (61%)	54.26	4.98	6.87	0.853	33.01	0,017
Configuration 5 (90%)	131.84	3.98	5.65	1.06	46.05	0.012

5. CONCLUSIONS

To study LOCA conditions closely, a new set-up is built focused on the characterization of two-phase flows with heat transfer in blocked structures at the representative sub-channel scale using specific instrumentation such as Laser Induced Fluorescence, Phase Doppler Anemometry and infrared thermography technics: A given vapor/droplet flow is injected into the heated tube; upstream and

downstream the droplet dispersed flow will be characterized using a PDA device (velocity, diameter, and PDF). Infrared thermography allows estimating the total wall to fluid heat transfer. Thanks to the Laser Induced Fluorescence device is possible to measure the temperature of the droplets and therefore estimate the sensible heat gained by the liquid. Using the measurement data, it will be possible to evaluate the coolability inside a blocked section.

A one-dimensional mechanistic model taking into account of the heat transfers mechanism in a post-dryout region is presented in this paper. This model allows estimating the respective impact of the different heat transfer mechanisms involved in the cooling of a heated tube by the two-phase non-equilibrium thermal flow. Three geometrical configurations of the partially blocked section have been analyzed in order to compare the axial distribution of each one of heat transfers mechanism: For all the cases, wall to vapor convective heat transfer is the most important contribution. Wall to fluid radiation contributions also has an important role. Even if wall to droplet direct contact heat transfer could be neglected, their consideration is important in situations where α_d is higher.

The present model is expected to be used in order to compare the results that will be obtained experimentally and thus better understand the phenomenon of cooling of a partially deformed section by a vapor/droplet flow. It is also expected to use these results in a wall heat transfer module with the aim of analyzing and predicting the change in wall temperature during the reflood phase by a vapor/droplet flow.

NOMENCLATURE

u	Velocity (m.s^{-1})
a_{int}	Volumetric interfacial area (m^{-1})
L_v	Vaporization latent heat (kJ.kg^{-1})
$\dot{G}$	Particle size change (m.s^{-1})
$\tilde{h}$	Enthalpy (J.kg^{-1}K^{-1})
Q	Heat transfer rate (W)
q	Heat transfer flux (W.m^{-2})
g	Gravitational constant (m.s^{-2})
C_p	Specific heat (J.kg^{-1}K^{-1})
n	Volumetric droplet concentration (m^{-3})
h	Heat transfer coefficient (W.m^{-2}K^{-1})
a	Absorption coefficient
T	Temperature (K)
S	Cross sectional flow area (m^2)
Pr	Prandtl number (-)
Nu	Nusselt number (-)
Re	Reynolds number (-)
α_d	Volumetric liquid fraction (-)
C_d	Drag coefficient (-)
B_T	Mass transfer number (-)
f_f	Friction factor (-)
t_r	Resident droplet time (s)
$\dot{m}$	Vapor mass flux (kg/s)
d_{oo}	Characteristic log-normal diameter (m)
d_d	Droplet diameter (m)
S_η	nth moment density
D_h	Hydraulic diameter (m)
z	Axial position (m)
L	Vertical tube length (m)

Greek symbols

ρ	Density (kg.m^{-3})
μ	Dynamic viscosity (Pa.s)
λ	Thermal conductivity (W.m^{-1}K^{-1})
ε	Emissivity (-)
γ	Surface tension (N.m^{-1})
σ_b	Stephan-Boltzmann constant (W.K^{-4})
σ	Standard log-normal deviation
φ	Gray body factor (-)
γ	Surface tension (N.m-^{1})

Subscripts

bal	Ballooned
d	Droplet
dep	Deposition
ev	Evaporated
nbal	Non-ballooned
sat	Saturation
v	Vapor
w	Wall
low	Lower bin limit
up	Upper bin limit

ACKNOWLEDGMENTS

This work is completed within the framework of RSNR Project from a French State aid managed by the National Agency for Research under the program of Investments for the Future carrying the reference n° ANR-11-RSNR-0017. Particular acknowledgments are also given to EDF for its financial support.

REFERENCES

[1] G. Repetto, M. Ch, B. Bruyère, T. Glantz, and S. Paul, "Core Coolability in Loss of Coolant Accident : the Coal Experiments," *WRFPM-TopFuel14, Sendai, Japan*, pp. 24–37, 2015.

[2] G. Repetto, C. Dominguez, B. Durville, S. Carnemolla, S. Paul, I. National, A. Lyon, F. Capelle, and V. Cedex, "the R & D Perfroi Project on Thermal Mechanical and Thermal Hydraulics Behaviors of a Fuel Rod Assembly During a Loss of Coolant Accident," pp. 1–14.

[3] A. Labergue, J.-D. Pena-Carrillo, M. Gradeck, and F. Lemoine, "Combined three-color LIF-PDA measurements and infrared thermography applied to the study of the spray impingement on a heated surface above the Leidenfrost regime," *Int. J. Heat Mass Transf.*, vol. 104, 2017.

[4] P. Lavieille, "Etude expérimentale du comportement aérothermique de gouttes en écoulement réactif ou non par utilisation de la fluorescence induite par laser à deux couleurs," 2001.

[5] A. Labergue, V. Deprédurand, A. Delconte, G. Castanet, and F. Lemoine, "New insight into two-color LIF thermometry applied to temperature measurements of droplets," *Exp. Fluids*, vol. 49, pp. 547–556, 2010.

[6] A. Bejan and D. Kraus, *Heat Transfer Handbook*. Whiley, 2003.

[7] R. Lee, J. N. Reyes, and K. Almenas, "Size and number density change of droplet populations above a quench front during reflood," *Int. J. Heat Mass Transf.*, vol. 27, no. 4, pp. 573–585, 1984.

[8] M. C. Yuen and L. W. Chen, "Heat-transfer measurements of evaporating liquid droplets," *Int. J. Heat Mass Transf.*, vol. 21, no. 5, pp. 537–542, 1978.

[9] C. H. Ban and Y. Kim, "Evaporation of a water droplet in high Temperature steam," *Journal of the Korean Nuclear Society*, vol. 32, no. 5. pp. 521–529, 2000.

[10] K. H. Sun, J. M. Gonzales-Santalo, and C. L. Tien, "Calculation of Combined Radiation and Convection Heat Transfer in Rod Bundles Under Emergency Cooling Conditions," *J. Heat Transfer*, vol. 98, no. 3, pp. 414–420, 1976.

[11] R. Siegel and J. R. Howell, "Thermal Radiation Heat Transfer, 3rd edition." p. All, 1992.

[12] Y. Guo and K. Mishima, "A non-equilibrium mechanistic heat transfer model for post-dryout dispersed flow regime," *Exp. Therm. Fluid Sci.*, vol. 26, no. 6–7, pp. 861–869, 2002.

[13] H. Li and H. Anglart, "Prediction of dryout and post-dryout heat transfer using a two-phase CFD model," *Int. J. Heat Mass Transf.*, vol. 99, pp. 839–850, 2016.

[14] S. A. Morsi and A. J. Alexander, "An investigation of particle trajectories in two-phase flow systems," *J. Fluid Mech.*, vol. 55, no. 2, p. 193–208., 1972.

[15] B. Oesterlé, *Écoulements multiphasiques : des fondements aux méthodes d'ingénierie*. Lavoisier, 2006.

[16] C. Morel, P. Ruyer, N. Seiler, and J. M. Lavieville, "Comparison of several models for multi-size bubbly flows on an adiabatic experiment," *Int. J. Multiph. Flow*, vol. 36, no. 1, pp. 25–39, 2010.

[17] A. M. Kamp, A. K. Chesters, C. Colin, and J. Fabre, *Bubble coalescence in turbulent flows: A mechanistic model for turbulence-induced coalescene applied to microgravity bubbly pipe flow*, vol. 27, no. 8. 2001.

[18] M. J. Meholic, D. L. Aumiller, and F. B. Cheung, "A comprehensive, mechanistic heat transfer modeling package for dispersed flow film boiling - Part 1 - Development," *Nucl. Eng. Des.*, vol. 291, pp. 302–311, 2015.